SAND2020-10542R

SAND20XX-XXXXR
LDRD PROJECT NUMBER: 220673
LDRD PROJECT TITLE: Stronger field-emission science via coupling novel nanoscale imaging techniques
PROJECT TEAM MEMBERS: Ezra Bussmann (PI), Taisuke Ohta, Barbara Kazanowska, George Wang, and Raj Tandon (PM)

ABSTRACT: We implemented a vacuum field emission electron microscope (FEM) using the electron optics of a low-energy /photoemission electron microscope (LEEM/PEEM). Historically, there have been other FEM hardware platforms, and the distinctive feature of our method is that it integrates with the LEEM/PEEM and associated techniques, enabling a powerful multi-capability toolset for studying fundamental materials properties underpinning field emission (FE) and vacuum arc initiation. Typically, LEEM is used to image surface structure, which influences both work function and electric field distribution near a surface, while PEEM is used to map photoelectric work function across a surface. Our FEM adds the capability for spatially-correlated coincident-site measurements of FE currents to go-along with structure and work function. LEEM, PEEM, and our FEM implementation achieve nanoscale spatial resolution relevant for materials studies in nanoscience/engineering. Our approach requires a straightforward calibration of the electron optics to enable focused FEM imaging under intentional electric field variation. We demonstrate the FEM approach by imaging field emitter arrays relevant for vacuum nanoelectronics. We demonstrate submicron spatial resolution and dynamic measurement of FE versus applied electric field. We anticipate this capability will enable fundamental structure-function studies of FE and arc initiation.

INTRODUCTION AND EXECUTIVE SUMMARY OF RESULTS: Electron emission from solid surfaces is a crucial mechanism in vacuum electronics, particle accelerators, and numerous other technologies.[1] Moreover, electron emission is an integral fundamental process in other more complex phenomena, e.g. vacuum arc initiation.[2] In regimes such as thermo-field emission, that are ubiquitous in research and technological contexts, emission rates depend exponentially on surface properties such as the work function , and the electric (*E*-) field concentration around surface structures, described by a field-enhancement factor, β.[3,4,5]

For realistic solid surfaces, ϕ and β are local surface properties that vary spatially owing to surface disorder.[6] Disorder that contributes to local ϕ and β includes roughness, polycrystalline microstructure,[7] adsorbates, nano- and microsized heterogeneities[8-10] including atomic steps,[11] surface reconstructions,[12] and dislocations terminated at the surface. Since electron emission rates depend strongly on local ϕ and β, the consequences of spatially patchy ϕ and β distributions are amplified and especially impactful in feedback-driven phenomena like arc initiation.

Predictive FE models, valuable to advancing several technologies, are maturing in computational power and sophistication to be comprehensive of microscopic materials properties that impact local ϕ, β, hence FE, and plausibly arc initiation. Both to enrich and validate such models, nanoscale-resolution microscopy of materials structure-to-FE relationships are relevant. Fig.1 shows an overview of a general strategy that we are pursuing through a sequence of Sandia projects to develop-test-improve predictive models for FE/arcs. In this strategy, spatially-resolved material properties measurements (e.g. ϕ, β, obtained via existing tools), are fed into a materials model, which is then used to simulate spatially resolved FE. An iterative feedback-improve loop is established by comparing model FE/arc predictions to experimental results to test model hypotheses, then revising models as new more detailed experimental data is available. To start, our hypothesis is that strong FE sites, identified by experiment and model, will serve as initiation sites for arcs.[2] Testing this hypothesis requires spatially-resolved methods for FE mapping (this work) and ultimately novel methods to map arc initiation sites (future work).

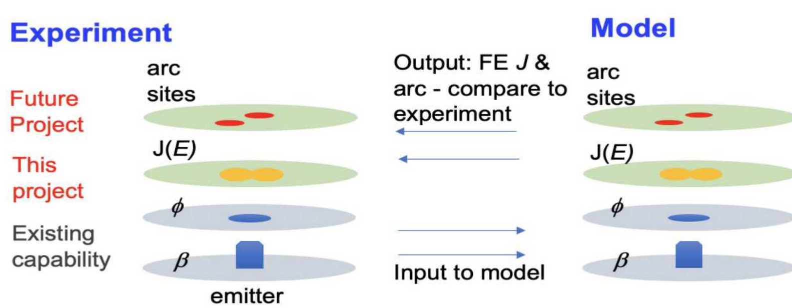

Figure 1 Strategy for improved models of field emission and vacuum arc initiation.

To image FE sites on surfaces, field emission electron microscopy (FEM) was created by Erwin Müller in 1936.[13] Figure 2 (a) shows a simple schematic diagram of Müller's FEM. It is conceptually similar to a cathode ray tube in an early television. By applying a sufficiently high E-field (>10^7 V/m) between a sample and a nearby phosphorescent screen, FE currents from the sample produce fluorescence on the screen, providing a spatially-resolved image of FE current from the sample surface. Müller-type FEM's achieved a spatial resolution ~ 2 nm in an arrangement that is suitable for imaging single point-like emitters.[13] Planar FE sources can also be imaged with FEM variants. More recently, scanning FEM (SFEM) techniques, Fig. 2 (b) have been demonstrated.[14] A drawback of SFEM is that it is a serial imaging technique that requires raster scanning a probe over the surface to collect an FE image. Also, the probe and sample are coupled in a near-field interaction, which leads to effects that are specific for the measurement apparatus, such as quantum mechanical field-emission resonances in the probe-sample gap.[14] Currently, neither FEM nor SFEM are commercially available, so researchers must build their own apparatus.

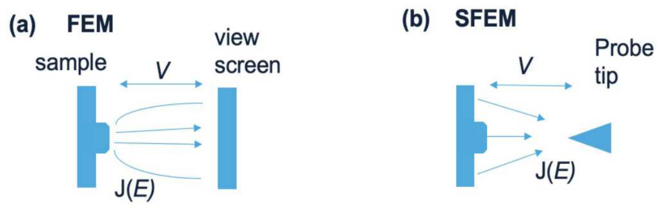

Figure 2 (a) A schematic of a field emission microscope (FEM). (b). A scanning FEM (SFEM)

Here, we describe a FEM implementation that integrates with our overall methods in Fig.1. Specifically, we utilized vacuum electron optics of a low-energy and photoemission electron microscope (LEEM/PEEM), one of the current techniques in our strategy, to image FE .[15,16] The approach requires straightforward calibration/compensation of the electron optics to accommodate variable *E*-fields. We find that our FEM is capable of imaging in tunable *E*-fields from ~0.5×10^7 to 5×10^7 V/m, and resolves emission sites with submicron resolution and a high sensitivity of ~10^{-3} A/m^2 Hz$^{1/2}$. We demonstrate FEM imaging on two types of structures. To characterize the electron optics and corrective compensation for variable *E*-field imaging, we used an array of micron-sized gallium nitride (GaN) field emitters of-interest for radiation-hard vacuum nanoelectronics. To investigate limitations of our FEM technique, especially near-field image distortion by surface protrusions, we studied a 10μm-sized carbon emitter used in bright electron sources of interest for microwave generation. The advantage of our approach is that techniques are nested *in-vacuo,* which is key to our approach to FE/arc science (Fig. 1). FE/arc-relevant materials properties, such as surface structure (β), ϕ , and composition, are mapped by a suite of coupled high-sensitivity atomic-and-nanoscale resolution techniques (LEEM, PEEM, X-ray photoelectron spectroscopy, scanning probe microscopy) to provide input information to FE/arc initiation models. The future impact of this work is to enable more accurate cost/risk mitigating computer-based design models of vacuum and high-voltage electronic devices used in a variety of national security mission applications.

DETAILED DESCRIPTION OF RESEARCH AND DEVELOPMENT AND METHODOLOGY: We have two key goals in this project: (1) to demonstrate a FEM capability that yields quantitative maps of FE current density *J* [amps/cm^2] with nanoscale spatial resolution, and (2) to vacuum-couple our FEM with other tools to integrate with the strategy outlined in Fig. 1.

The electron optics of our FEM is a *LEEM III* from *Elmitec Elektronenmikroskopie GmbH* in Clausthal, Germany.[15.16] In the apparatus, Fig. 3, FE is driven by a tunable high *E*-field (0.5-2x10^7 V/m) established by applying a tunable high voltage (*HV*) = -10, -15, -20 kV to the sample("specimen" in Fig. 3), with the sample situated at a tunable millimeter-scale working distance, *z =0.3-3 mm*, near a grounded electromagnetic (EM) objective lens that is the input to the electron optics. The *E*-field, *HV*/*z*, can be tuned by adjusting the *HV* or *z*. A series of electromagnetic lenses project the FE electrons onto an electron multiplier (multichannel plate, MCP). The output of the MCP is projected on a phosphorescent viewscreen. Images are acquired using a PC-interfaced video camera (not shown) focused on the viewscreen.

There are two main challenges to develop a useful FEM capability in the context of the electron optics described above. To calibrate the view screen image intensity to a quantitative current density, *J* [amps/cm^2] is challenging because there is not a straightforward route to access the electron beam path to measure, e.g. with a Faraday cup and ammeter, the extremely small total currents (<10^{-9} A) anticipated from typical nanostructures of-interest at *E*-fields attainable in the tool. Second, when characterizing a material's FE properties, it is common and useful to measure *J* as a function of varying applied *E*-field. Varying the *E*-field requires that the LEEM optics be calibrated to compensate for varying *HV* or *z*. When the *E*-field is varied, the image focus, magnification, and orientation all change owing to various EM effects (Lorentz force) in the electron optics.

We calibrate viewscreen intensity to *J* [amps/cm^2] by reflecting an electron beam of known total current (100 nA) from the sample and recording the image intensity versus beam diameter on the viewscreen.

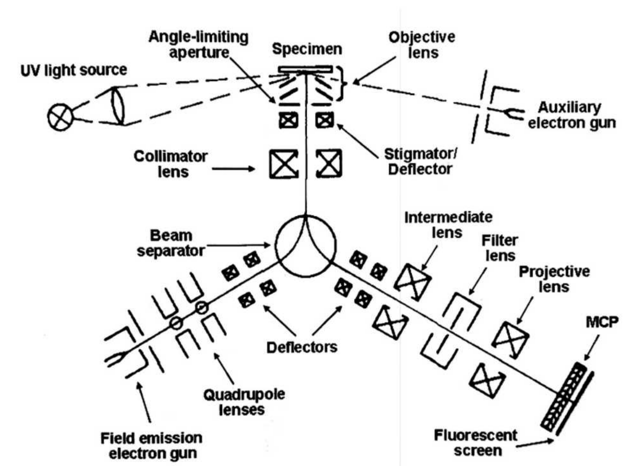

Figure 3 A schematic of electron optics for a low-energy electron microscope, and photoemission electron microscope (LEEM/PEEM), that we have utilized for FEM. The electron guns are used for LEEM, and they turned off during FEM studies.

The calibration that we measure for our mode of operation, which is highly dependent upon the tool operating parameters, is 6(±1) x10^{-4} [A/m^2] for an image field of view of 150µm and an image acquisition time of 0.1s. In presenting our results in subsequent figures, we have calibrated the image intensity to J [amps/cm^2] where it is relevant to do so. The accuracy of this method depends upon the transmittance of the electron optics, which is known to be ~100% for similar apparatus [Elmitec, private communication].

To vary the *E*-field, it turns out to be most convenient to tune *z,* while *HV* is held constant. To maintain a focused image, it is straightforward to compensate the change in z by changing the objective strength (current). This scenario is qualitatively similar to a compound optical microscope, where magnification and objective focal length are connected with working distance. For *HV*=15 keV, the objective current, I_{obj}, must be set to 1350 mA for z = 2mm, then changed at a rate $\Delta I_{obj}/\Delta z$ = 190±10 A/m to maintain a focused image (for *z* in the range 0.3-3 mm). The z-I_{obj} relationship is nearly linear for millimeter scale variations in z.

To optimize the optics compensations for variable *E*-field imaging, we utilize an array of submicron-sized gallium nitride (GaN) field emitters. Figure 4 shows images of a single GaN emitter from a regular square array on a 20μm pitch. GaN FE arrays are prepared from planar GaN by an anisotropic chemical etch. GaN is grown by metalorganic chemical vapor deposition (MOCVD) in a Taiyo Nippon Sanso SR4000HT reactor on 2-inch c-sapphire substrates, with n-type doping using Si at a concentration of 3x10^{18} cm^{-2}. The wafers were diced into uniform 6mm by 8mm coupons, with the 8mm edge oriented parallel to the wafer flat. Arrays of 1.3um dimeter dots were patterned in PMMA A4 photoresist using electron beam lithography (EBL) in the JEOL system. Following development, a metal mask consisting of Ti/Ni was deposited to a thickness of approximately 180nm, with the first 5 nm being Ti to promote mask adhesion. An inductively coupled plasma reactive ion etch (ICP-RIE) of Cl_2/Ar/BCl_3 chemistry with flows of 50/25/5 sccm, respectively, at a chamber and chuck temperature of 65 °C, was used to etch the initial nanowire structures to a depth of ~1.8µm. The elevated chuck and wafer temperatures are required to increase surface reaction volatility to aid in etch byproduct removal and prevent self-masking which negatively results in surface whiskering. The remaining metal mask was removed in piranha etch for 10 minutes to fully clean the sample surface, which was followed by a 2 minute buffered oxide etch (BOE) to remove any oxide. Immediately after BOE, the sample was etched in a hot, 120 °C H_3PO_4 bath for 20 minutes yielding pointy, hexagonal, nanowires, as shown in Fig. 4. The sample is transferred through air to the FEM (P≤10^{-9} torr) where it is annealed (T~500^{o}C), which is found to improve both the FE intensity and stability, presumably by removing some weakly-adsorbed contaminants.

To characterize the FE image distortions caused by field enhancement around protrusions, we utilize 10-μm-scale carbon FE structures (C posts, supplied by Air Force Research Labs) grafted to a Pt substrate.[17] The C posts are ~30μm diameter carbon fibers (commercially available). Using focused ion bombardment (FIB), a ~50μm length of fiber was cut to form a small cylindrical post, Fig. 4, that was welded to a Pt substrate in a vertical orientation. The Pt provides a flat clean equipotential surface with a work function (5.2-5.7 eV) to support the post. To mitigate weakly-adsorbed contaminant prior to experiments, the sample was annealed (T~200^{o}C) in the FEM vacuum (P≤10^{-9} torr), which has minimal impact on the measurement outcomes.

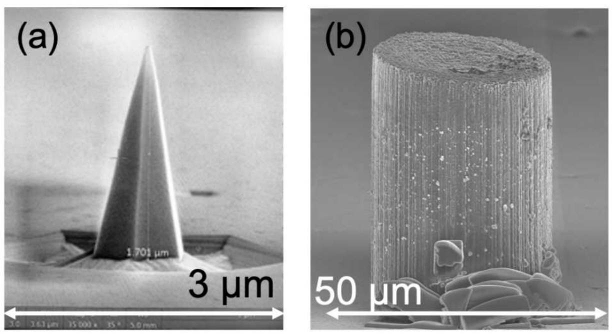

Figure 4 (a) Scanning electron microscope images of (a) a GaN field emitter in an array, and (b) a carbon field emitter post (C post) (courtesy of Air Force Research Labs).

RESULTS AND DISCUSSION: We begin by demonstrating our FE imaging technique with a study of GaN FE arrays, proceed to describe image distortions when using our FEM on larger protrusions (C posts from AFRL), and conclude by identifying limitations to our approach and by providing the path forward toward the comprehensive understanding of the field emission process.

We use PEEM to locate structures-of-interest for FEM imaging. PEEM is performed by illuminating a sample with a Hg arc lamp with a spectral range out to hν ~ 4.1 eV (λ~300 nm). An image of photoemitted electrons is projected to the viewscreen. A PEEM image of a GaN FE array is shown in Fig. 5 (a). The UV illumination is from the lower right at an angle about 17^{o} above the sample surface, leading to an asymmetric bright-dark appearance owing to shadowing effects. The emitters appear intensely bright on one side owing to near normal-incidence illumination of one face of the emitters, whereas they are dark (shadowed) on the opposite side.

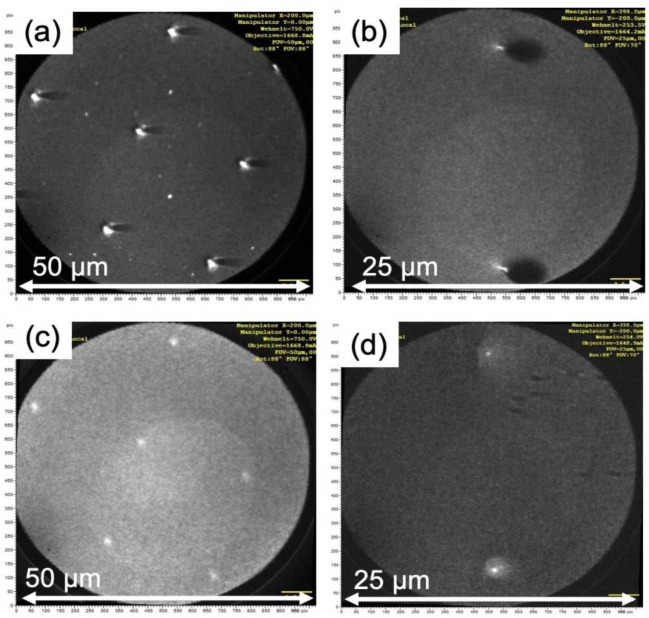

Figure 5 (a,b) PEEM, and (c,d) FEM images of the GaN emitter array.

Having located the FE array, the Hg light source is removed, and the FEM chamber is shuttered against stray light to prevent photoemitted electrons from contributing significantly to image intensity. Figure 5 (b) shows an image of the GaN FE array after removing the Hg lamp. By contrast to Fig. 5 (a), the emitters appear radially symmetric sans illumination, *i.e.* there is no shadowing effect. The observed electron intensity that is strongly associated with field-enhancing GaN structures in the presence of a strong *E*-field (10^7 V/m) and without any other obvious excitations (UV light, intentional electron or ion bombardment) is the first indication that field emission is likely to be dominating image contrast.

Besides FE, some other possible unintentional excitations that could produce image intensity are secondary electron emission owing to thermionic emission, stray light in the chamber, spurious ion, and/or electron bombardment. In contrast to our observation of bright electron emission from the FE array, image contrast dominated by *secondary* electron emission due to spurious electron bombardment and (unlikely) negative ion bombardment, would cause the GaN emitters to appear relatively dark, owing to the higher local field *repelling* the spurious primary electrons/ions from the emitters. Image contrast from secondary electrons by spurious positive ion bombardment (e.g. from ionized gas), could cause the emitters to appear bright, but significant bombardment is unlikely at the pressures ($\leq 10^{-9}$ Torr) in the FEM.

A second key observation that is consistent with image intensity dominated by FE, is the exponential increase of the intensity as the working distance, *z*, is decreased. FE is expected to follow a Fowler-Nordheim equation (FNE) wherein the FE *J* is an exponential function of the applied (mean) *E*-field, so we expect exponential increases of image intensity with decreasing *z*. Figure 6 shows images recorded as a function of *z*. The total intensity of the images, as well as intensity local to the individual GaN spikes , increases considerably as the gap is reduced and the *E*-field increases. The intensity from a spike versus *E*-field (*z*) is plotted in Fig. 6, in a Fowler-Nordheim form and follows the expected exponential form consistent with FE. To further substantiate the viewpoint that image intensity is dominated by FE, we tested the thermionic emission characteristics of the GaN array. Owing to the 3.4eV bandgap of GaN, we find a negligible change in image intensity for T<300°C. For T>300°C, thermionic contributions to FE (thermo-field emission) becomes appreciable, and the image intensity and contrast increase. In summary, the observations described in the preceding two paragraphs strongly support the hypothesis that FE is the dominant contrast mechanism in Figs. 5 and 6.

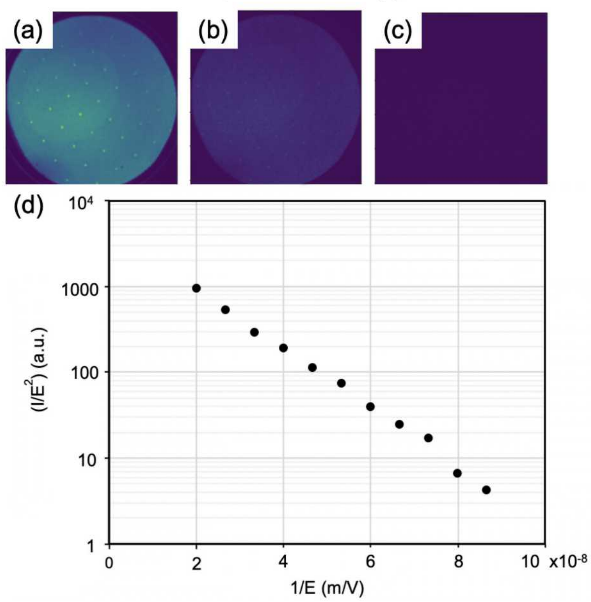

Figure 6 (a-c) FEM of GaN emitter array at HV=15 kV, and z=2, 1.4, and 1 mm respectively. The image diameter is 150 µm. (d) A Fowler-Nordheim plot of image intensity (current density) for a small region of the image

Our FEM is capable of submicron resolution (a key project success). Resolution limits in our FEM, are determined by two main effects. First, FE electrons have lateral velocity components (orthogonal to the axis of the imaging apparatus) due to the shape of the local field distribution around an FE structure and thermionic emission. Second, a 3D spray of FE electrons is then projected forward to the 2D viewscreen, leading to convolution effects when imaging extruded structures of the type that we are using. For the GaN spikes, the approximate radius at the base of the spike is around 500 nm, see Fig. 4 (a), and we expect a similar length scale to resolve a single emitter. And indeed, we find that the transition (10% to 90% of full signal) of a single-emitters FE spot is around 500 nm, Fig. 5 (e).

Although our FEM resolves submicron FE structures, field distortions along with the 3D-to-2D projective imaging, create practical challenges to resolving local submicron structures on larger structures with 3D geometries. For example, when imaging the C posts in Fig. 4 (b), the resolution of our method is significantly impacted by field distortion, which is approximately on the same length scale of the emitter. Figure 7 shows a few images of the C posts, and it is clear that submicron resolution is not achieved. Also, the focusing of electrons from the top of the emitter post is substantially different from the bottom, leading to a convolution of intensity from various sources.

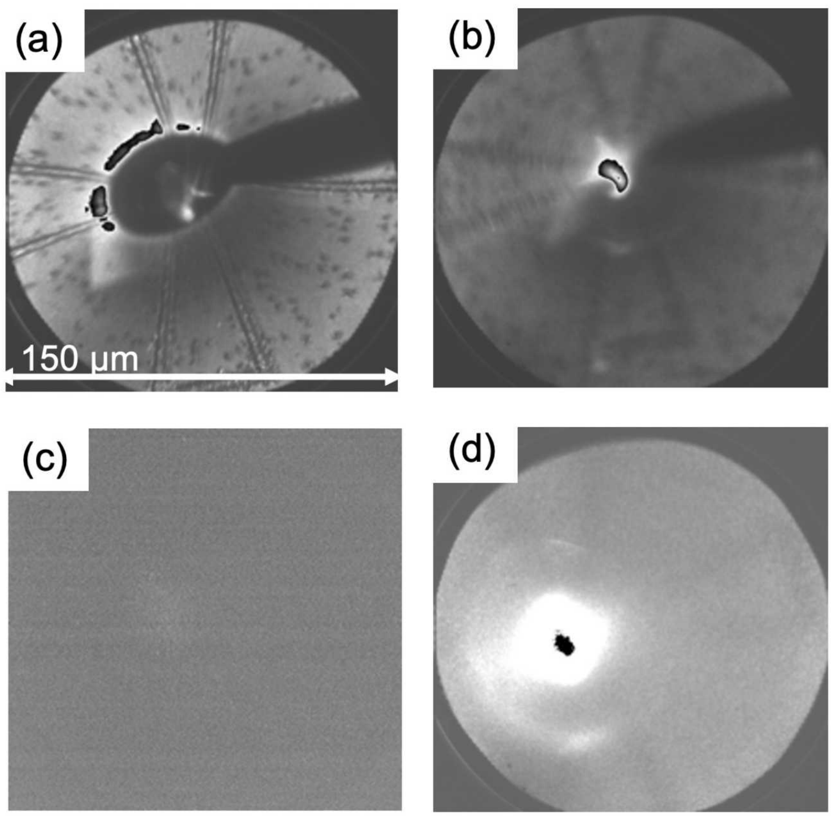

Figure 7 (a,b) PEEM images of C post emitter with HV=15keV, and z=2mm, for (a) the objective focused on the substrate, and (b) the objective focused on the tip of the emitter. Subsequently, the UV lamp was removed, and (c,d) the C post was imaged with the focus on the emitter tip with z=1.3 mm and z=0.3 mm. Dark patchy regions are areas where the intensity is outside of the dynamic range of the imaging apparatus.

ANTICIPATED OUTCOMES AND IMPACTS: From a programmatic and technical standpoint, our next steps will be to integrate our new FEM capability into our strategy for comprehensive FE/arc science, as illustrated in Fig. 1. The long-term impact of this work will be to add to a cost-cutting and risk-mitigating strategy in developing new electronics technologies for mission applications. For several DOE/NNSA/Sandia programs, the current paradigm for high voltage and vacuum electronics design is often empirical protyping/testing, with slow and expensive learning cycles. A predictive computational design model, implemented in Sandia's EMPIRE software via separate funding sources, would significantly mitigate time/cost/risk in creating new products. As indicated in Fig.1, our new capability is integral to a comprehensive strategy to improve FE/arc science models. Prior to this project, Sandia had no comparable tool relevant to fit into this strategy.

Through this LDRD, we developed a few follow-on funding paths that include 2 new projects with nuclear deterrence (ND) mission, one potential strategic partnership project (SPP) opportunity with Air Force Research Labs, and an avenue for potential impacts to another current LDRD (Project 213061, GaN Vacuum Nanoelectronics: A New Platform for Radiation-Hard Devices and Beyond, P.I. George Wang)

Near term, the FEM capability will be leveraged toward ND mission thru direct-funded FY21 follow-on projects. The first Sandia/NNSA Mission projects for our FEM are to examine FE and related properties of surfaces in vacuum devices that include sprytron switches and neutron generators. For these devices, engineering control over arc initiation is critical, and surface FE is thought to play a role in initiation. Overall, the projects will include the full suite of elements shown in Fig. 1. We will use the new FEM to test predictions against experiment.

A second anticipated near-term application, via a collaboration with Air Force Research Labs with direct mission relevance, that we will pursue in FY21 is to bright FE electron sources used in directed-energy applications. A single emitter is shown in Figs. 4 (b) and 7. The FEM will be used toward fundamental studies of individual and multiple emitters. The anticipated impact is to provide measurements that serve as a basis to model interactions between FE structures in large dense arrays. In this context, screening interactions between emitters is a significant concern []. The FEM will be used to directly image interactions. The anticipated impact is to improve models describing the screening interactions, which will contribute to fundamental understanding required to design brighter and more efficient electron sources.

This project has resulted in potential Intellectual Property (IP). It may be possible to obtain an improvement patent covering our new application of the existing *Elmitec* LEEM optics for FEM.

We will submit a Sandia Technical Advance (TA) covering our FEM implementation.

We will publish a journal article describing the work in an appropriate peer-reviewed venue such as *Journal of Applied Physics*. In addition, we will present a contributed abstract and talk at an appropriate venue such as *American Vacuum Society Symposium*. Both the description of the new FEM platform, such as the necessary compensations for variable field imaging, and the spatially resolved studies of GaN field emitters will assist other researchers, both in FE science and engineering of semiconductor vacuum nanoelectronics.

From a technical standpoint, there are several important steps forward that we will demonstrate during follow-on projects. First, we note several improvements to be made to the FEM capability. Second, we describe an integrated platform for arc tests for ultimate completion of the strategy outlined in Fig. 1.

We will do the following key next steps to improve our FEM capability: (1) improve image quantification, i.e. calibration of intensity to [amps/cm^2], (2) increase measurement bandwidth (speed), (3) increase the accessible range of *E*-fields, and (4) to create a FE image deconvolution model to make sense of the 3D-to-2D projected image. Briefly, we will use a straightforward Faraday cup technique to improve calibration of intensity to [amps/cm^2]. We will increase the measurement bandwidth by increasing the sensitivity of the electron multiplier, which is risky because the multiplier can be damaged under some conditions. We will increase the range of accessible *E*-fields (currently limited by arcs between the objective and sample) by lowering the base pressure ($<3 \times 10^{-10}$ Torr) in the FEM and applying higher HV and lower gap. And finally, we will implement a 2D-to-3D image deconvolution model using EMPIRE under direct-funded mission work in FY21.

Finally, looking beyond FY21, we will take the essential final step to realize our comprehensive FE/arc science strategy, by creating/integrating a tool to perform arc experiments that is vacuum-coupled to the FEM. This tool will allow to compare predictions from models, built from unprecedented detailed materials descriptions, directly with experiments. We will use this capability to move EMPIRE arc initiation simulations from a qualitative to a quantitative predictive tool for vacuum electronics design.

CONCLUSION: We demonstrated the field emission imaging capability utilizing the electron optics designed for LEEM/PEEM. Our FEM achieves ~500 nm spatial resolution and sensitivity of 0.001 amps/m^2 Hz$^{1/2}$. The resolution and sensitivity are relevant for future studies regarding vacuum electronics. The advantage of our approach is that several techniques are then naturally nested *in-vacuo*. This nesting enables our approach to fundamental FE/arc science, shown in Fig. 1. Specifically, FE/arc-relevant materials properties, such as surface structure (β), work function (ϕ), and composition, and can be imaged by a suite of coupled high-sensitivity atomic-and-nanoscale resolution techniques (LEEM, PEEM, X-ray photoelectron spectroscopy, scanning probe microscopy) to provide input information to FE/arc initiation models (EMPIRE). The impact of this work will be to enable cost/risk mitigating computer-based design models of vacuum and high-voltage electronic devices used in a variety of national security mission applications.

REFERENCES

1. K. L. Jensen, IEEE Transactions on Plasma Science 46 (6), 1881-1899 (2018).
2. R. L. Boxman, D. M. Sanders and P. J. Martin, Handbook of vacuum arc science & technology: fundamentals and applications. (William Andrew, 1996).
3. R. H. Fowler and L. Nordheim, Proceedings of the Royal Society of London. Series A, Containing Papers of a Mathematical and Physical Character 119 (781), 173-181 (1928).
4. R. G. Forbes and J. H. Deane, Proceedings of the Royal Society A: Mathematical, Physical and Engineering Sciences 463 (2087), 2907-2927 (2007).
5. K. L. Jensen, Journal of Applied Physics 126 (6), 065302 (2019).
6. R. G. Forbes, Solid-State Electronics 45 (6), 779-808 (2001).
7. J. Lecoeur, J. Bellier and C. Koehler, Electrochimica acta 35 (9), 1383-1392 (1990).
8. R. Vanselow and X. Li, Surface science 264 (1-2), L200-L206 (1992).
9. R. Smoluchowski, Physical Review 60 (9), 661 (1941).
10. R. Strayer, W. Mackie and L. Swanson, Surface Science 34 (2), 225-248 (1973).
11. K. Besocke, B. Krahl-Urban and H. Wagner, Surface Science 68, 39-46 (1977).
12. G. A. Haas and R. E. Thomas, Journal of Applied Physics 40 (10), 3919-3924 (1969).
13. E. W. Müller, Z. Physik **106**, 132 (1937).
14. RS Becker, JA Golovchenko, EG McRae, BS Swartzentruber, Physical Review Letters 55, 2028 (1986).
15. E. Brüche: Elektronenmikroskope, Naturwissenschaften 20, 49 (1932)
16. E. Bauer: LEEM and UHV-PEEM: A retrospective, Ultramicroscopy 119, 18–23 (2012)
17. W. Tang et al. *Journal of Vacuum Science & Technology* **B** 30, 061803 (2012)